Distributed Feedback Lasers Based on Green Fluorescent Protein and Conformal High Refractive Index Oxide Layers

Markus Karl, Andrew Meek, Caroline Murawski, Laura Tropf, Changmin Keum, Marcel Schubert, Ifor D. W. Samuel, Graham A. Turnbull, and Malte C. Gather*

Fluorescent proteins have emerged as an attractive gain material for lasers, especially for devices requiring biocompatibility. However, due to their optical properties, integration with distributed feedback (DFB) resonators is not readily achievable. Here, a DFB laser with enhanced green fluorescent protein (eGFP) as the gain material is demonstrated by incorporating a thin (65 nm), high refractive index ($n = 2.12$) ZrO_2 interlayer as waveguide core. Deposition of ZrO_2 via atomic layer deposition yields a smooth and conformal film as required to minimize optical losses. Lasing emission is obtained from 2D second-order DFB eGFP lasers at pump power densities above 56.6 kW cm^{-2} and a wavelength tuning range of $\Delta\lambda = 51.7$ nm is demonstrated. Furthermore, it is shown that in contrast to conventional organic DFB lasers, both transverse electric (TE) and transverse magnetic (TM) modes are accessible. The effective refractive index of these modes can be predicted accurately through optical modelling. Using far-field imaging, the laser beam profile is studied and TE and TM modes are distinguished.

1. Introduction

Green fluorescent protein (GFP) was first discovered and extracted from the jellyfish *Aequorea victoria* in the North Pacific, and is now commonly used as a marker for genes and molecules in biology laboratories around the world.[1,2] This widespread use has gone hand-in-hand with extensive research into finding new fluorescent proteins and making further optimizations to existing ones.[3,4] Today, there is a remarkable library of different fluorescent proteins with spectral bands covering the whole visible

spectrum, providing optical gain on a par with state-of-the-art fluorescent polymers.[5,6] Furthermore, the barrel-like structure of many fluorescent proteins protects the active fluorophore in the center of the protein from self-quenching,[5] which in turn leads to excellent fluorescence properties in solid-state films. While the production of fluorescent proteins is currently still expensive, the use of biosynthesis offers the attractive prospect of being able to produce large amounts of protein in a low-energy process and without the need for organic solvents and other environmentally demanding substances.

Due to their biocompatibility, light-emitting properties, and potentially more sustainable synthesis, fluorescent proteins also received attention from the laser community and lasers based on fluorescent proteins with a variety of resonator structures have been demonstrated. Two remarkable milestones are the biological single-cell laser, in which enhanced GFP (eGFP)[7] is used as the gain material, and the fabrication of a low threshold polariton laser based on eGFP that emits laser-like radiation from a quasi-Bose–Einstein condensate of exciton-polaritons.[8] In the context of solid-state lasers, a further advantage of using fluorescent proteins is that their barrel-like molecular structure reduces exciton–exciton annihilation, thus delaying the onset of gain saturation at high excitation densities.[8]

Distributed feedback (DFB) grating resonators are an attractive class of resonators because they can be operated at low thresholds and in a single mode regime and because they comprise a planar waveguide structure that can be fabricated on large scales, with high reproducibility.[9–11] However, their integration with eGFP as gain material is not straightforward due to the relatively low refractive index of the protein. Recently, a device incorporating a mixture of eGFP and silk as gain material deposited on top of a DFB resonator has been demonstrated.[12] However, lasing thresholds have remained high and the emission properties of the devices were not fully understood.

Atomic layer deposition (ALD) is a chemical vapor deposition method, in which a thin film of material, typically a metal oxide, is grown one atomic layer at a time, making it possible to precisely control the layer thickness.[13] Since ALD relies on chemical reactions, conformal layers can be grown on substrates with complex topographies including grating structures. The process usually

Dr. M. Karl, A. Meek, Dr. C. Murawski, Dr. L. Tropf, Dr. C. Keum,
Dr. M. Schubert, Prof. I. D. W. Samuel, Prof. G. A. Turnbull,
Prof. M. C. Gather
Organic Semiconductor Centre
SUPA
School of Physics and Astronomy
University of St Andrews
St Andrews KY16 9SS, UK
E-mail: mcg6@st-andrews.ac.uk

**ADVANCED
SCIENCE NEWS**

www.advancedsciencenews.com
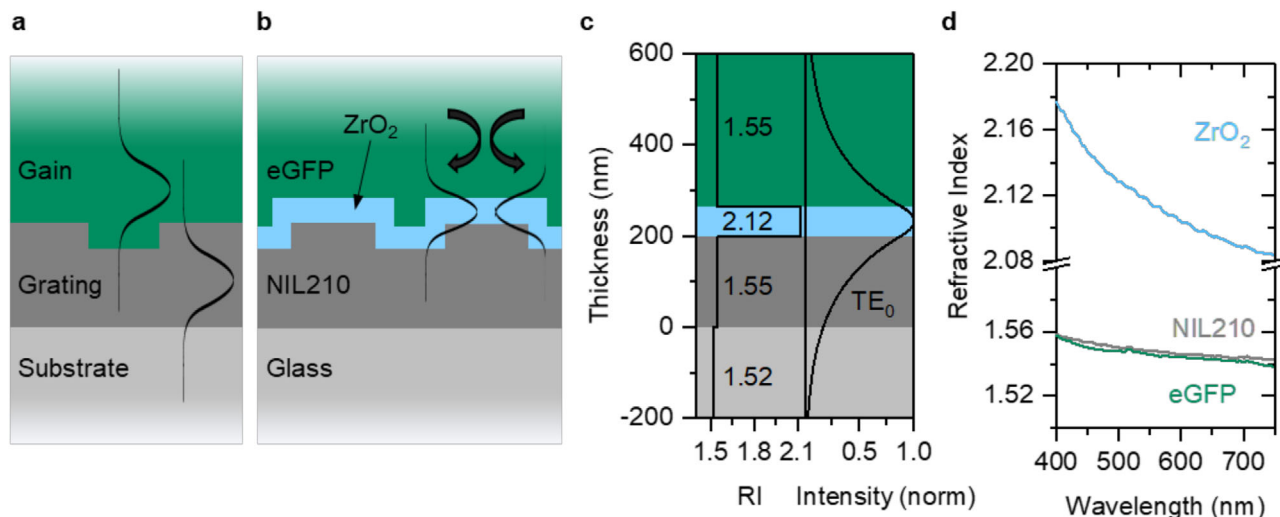
LASER
&PHOTONICS
REVIEWS

www.lpr-journal.org

Figure 1. Design of a DFB laser based on eGFP as gain material. a) Illustration of a conventional DFB waveguide structure consisting of a substrate, a grating-containing layer, a gain layer, and air above. Depending on the refractive index of the different layers, the gain layer can either form the waveguide core or the waveguide cladding (as schematically illustrated for the TE_0 mode). b) Schematic cross section through the DFB structure used here, incorporating a grating layer made of the UV-curable polymer resist mr-NIL210, a high refractive index metal oxide waveguide core layer of ZrO_2 that confines the photonic modes, with an evanescent component extending into the eGFP gain layer above. Mode profiles for illustration only. c) Refractive index profile and actual, modeled TE_0 mode profile at 530 nm for the same structure as in (b). d) Wavelength-dependent refractive index of eGFP, the UV-curable polymer resist mr-NIL210, and ZrO_2.

relies on the use of two different precursor materials that react with the surface one at a time in a sequential and self-limiting manner. The repetitive use and reaction of the two precursors leads to the slow growth of a thin film. ALD is commonly used to produce the gate dielectric in transistors,[14] encapsulate organic light-emitting diodes,[15] and for surface modifications of complex nanostructured materials,[16] but it has not previously been used to define DFB gratings for lasers.

Here, we show how bulk eGFP can be used as a solid-state gain material in an optimized 2D second-order DFB resonator structure to obtain low-threshold lasing emission from different modes over a broad spectral range. Fluorescent polymer-based DFB lasers often incorporate the fluorescent polymer gain layer as the waveguide core, with a further polymer or silicon dioxide layer with an inscribed DFB grating forming the waveguide cladding. As the low refractive index of eGFP would prevent waveguiding in such a structure, we incorporated a thin, high-index metal oxide layer of a controlled thickness (65 nm) that is produced with ALD and that confines the light close to an eGFP-based gain layer. Furthermore, we study the polarization and far-field emission from the lasers and identify distinctive transverse electric (TE) and transverse magnetic (TM) lasing modes from these DFB eGFP lasers.

2. DFB eGFP Laser Design and Fabrication

Figure 1a–c schematically illustrates the structure and refractive index profile of the DFB laser. The structure contains a multilayer slab waveguide to confine light within the plane, a grating formed in a UV-curable polymer resist, and the eGFP gain medium as a cladding layer located in proximity to the grating. For a DFB laser to work effectively, it is important that the transverse lasing mode supported by the structure overlaps significantly with both the gain medium and grating, and that the refractive index contrast at the grating surface is sufficiently high. In general, depending on the refractive index of the individual layers forming the DFB laser, the gain layer can be located either in the core or the cladding of the DFB slab-waveguide structure. The first option is often overall more desirable as it maximizes modal overlap with the gain layer. However, the thickness of the waveguide core must be controlled precisely, and a smooth film morphology is required to minimize optical loss from surface scattering. In addition, a cladding layer with an inscribed grating and a lower refractive index than the gain medium is required, which is challenging in our case given the refractive index of eGFP is only around 1.55 (see below). The other option, in which the mode is confined in the cladding layer, relies on evanescent gain that is provided by the overlap of the evanescent part of the waveguided mode and the gain region.[17,18] While this approach reduces the available modal gain, it has the advantage of relaxing the requirements on the thickness homogeneity and refractive index of the gain layer.

Using spectroscopy ellipsometry, we measured the optical constants of films of neat eGFP and the UV curable polymer resist used in this work (mr-NIL210). At the optimum lasing wavelength of eGFP ($\lambda = 530$ nm) the refractive indices of the two materials were found to be identical within the accuracy of the measurement ($n \approx 1.55$, Figure 1d). As a result of this similarity in refractive index, one would expect that it is not possible to obtain sufficient Bragg scattering and robust waveguiding with a simple stack formed by the two materials.

In order to form a waveguide structure with sufficient refractive index contrast between grating and gain material, we modified the laser stack by introducing a thin layer of a transparent high refractive index metal oxide (ZrO_2, $n = 2.12$, Figure 1d) at

**ADVANCED
SCIENCE NEWS**

www.advancedsciencenews.com
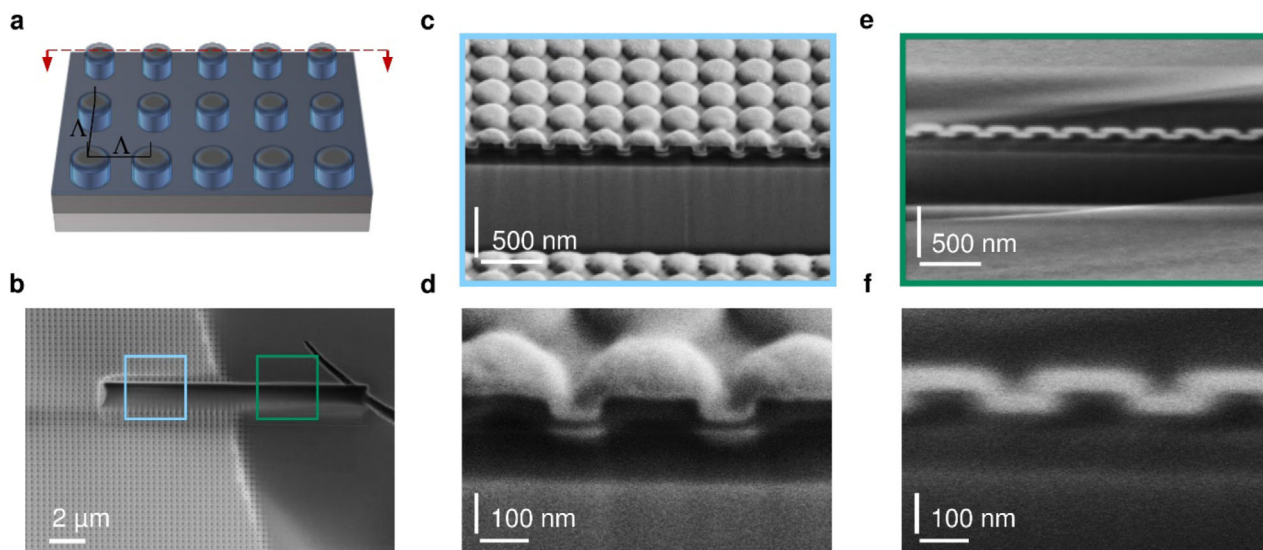
**LASER
& PHOTONICS
REVIEWS**

www.lpr-journal.org

Figure 2. Grating characterization. a) Illustration of a DFB eGFP laser based on a 2D second-order grating (dark gray) with a thin metal oxide layer (blue) on top. The grating period Λ is defined as the distance between two grating columns. For clarity, the eGFP film is not shown. The red dashed line indicates the position of the cross sections shown in (c–f). b) Top-view SEM image of a 2D second-order grating partially covered with eGFP (right half of image), incorporating a trench-cut through the individual layers that was formed via FIB milling. c) 52° glancing incidence SEM image of a grating section not covered with eGFP (corresponding to blue square in (b)). The layers can be identified as ZrO_2 (bright), grating polymer (dark), and glass substrate (slightly bright), top to bottom. d) Close-up of the structure shown in (c). e) Glancing incidence SEM image of a grating section covered with eGFP (dark top layer) (corresponding to green square in (b)). f) Close-up of the structure shown in (e).

the interface between gain material and grating resist. Figure 1c shows the refractive index profile across the DFB laser stack comprising a carrier glass substrate, the nanoimprint resist, a thin layer of ZrO_2 covering the grating and acting as the waveguide core, and eGFP as the gain material. The figure also shows the calculated TE_0 mode profile ($\lambda = 530$ nm) in the stack for a mr-UV210 layer thickness of 200 nm and a ZrO_2 layer thickness of 65 nm. As discussed above, the use of a nonemissive waveguide core requires an evanescent pumping scheme. However, we found that for the small layer thickness of the high refractive index material used here, the modal overlap factor Γ with the gain layer can be as large as 31%, and that this is sufficient to provide low-threshold lasing. We note that for such a configuration, the evanescent component of the mode extends by over 300 nm into the gain layer. Therefore, selecting a gain layer thickness substantially larger than this is advisable to avoid any impact of thickness inhomogeneity on the device characteristics.

Based on this waveguide structure, we fabricated the DFB eGFP laser structures schematically shown in **Figure 2**a using a combination of solution processing, UV nanoimprint lithography (UV-NIL), and ALD. To assess the quality of the laser structures, we milled a trench through the stack using a focused Ga ion beam and imaged the structure with a scanning electron microscope (SEM). Figure 2b shows a top view SEM image of a 2D second-order $\Lambda = 330$ nm grating that was partially covered with eGFP. The bright left-hand part of the image shows the uncoated grating, whereas on the darker right-hand side, the grating is covered with a solid-state eGFP film and therefore the grating columns are not visible. Figure 2c,d (close-up) shows a glancing incidence SEM image of the uncovered grating section. The polymer grating columns can be identified as the dark periodic structure ($\Lambda = 330 \pm 10$ nm, standard error of mean) sitting on a

residual continuous polymer layer with a thickness of 149 ± 6 nm. Each grating column is 198 ± 7 nm wide by 72 ± 4 nm tall and the grating fill factor is $60\% \pm 5\%$. The bright, smooth area underneath the polymer grating is the top surface of the carrier glass slide that stopped the milling of the focused ion beam (FIB). The bright layer on top of the polymer grating is the ZrO_2 layer; in the SEM image, this appears to form a half-dome-shaped cover with inhomogeneous thickness across the grating columns. However, glancing incidence SEM images of grating regions covered with eGFP demonstrate that the ZrO_2 layer does in fact form a conformal layer of constant thickness, and thus reproduces the periodic grating structure (Figure 2e,f (close up)). This is expected for a layer formed by ALD, in which the growth process relies on a self-limiting chemical reaction. The ZrO_2 layer also appears sharper in regions of the sample where it is covered with eGFP which is due to rejection of out-of-focus ZrO_2 signal in the background (see Figure 2d). The ZrO_2 thickness measured from the SEM image is 67 ± 4 nm (taking sample tilt into account), close to the nominal thickness of 65 nm. Hence, the FIB/SEM images confirm that the fabrication of our DFB eGFP laser structure worked as anticipated.

3. Optical Characterization of DFB eGFP Lasers

Next, we optically characterized the DFB eGFP lasers using a custom-built inverted fluorescence microscope. **Figure 3**a shows input–output characteristics of the structures when optically excited with ns pulses from an optical parametric oscillator (OPO) that was tuned to the absorption maximum of eGFP (490 nm). Above a threshold input power fluence of 57 kW cm^{-2}, we observed a superlinear increase in output power. This is a first
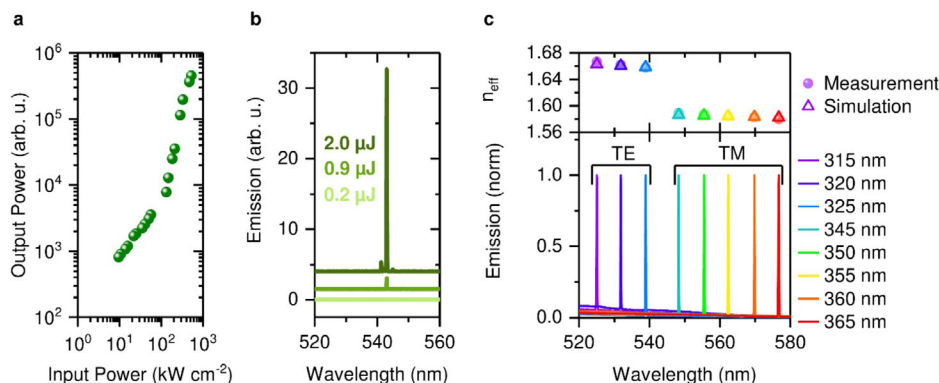
Figure 3. Laser characterization. a) Input–output characteristics of a DFB eGFP laser based on a 2D second-order grating with a period $\Lambda = 330$ nm and a thin ZrO_2 layer with a thickness of 67 ± 4 nm. The lasing threshold for this device is 56.6 kW cm^{-2}. b) Emission spectra for the same DFB eGFP laser for input pump power densities below, just above, and well above threshold (spectra vertically shifted for clarity). c) Bottom panel: Emission spectra for DFB eGFP lasers with different grating periods. The individual lasing modes are labeled with their respective polarization (TE or TM). Top panel: Effective refractive mode index n_{eff} corresponding to the individual lasing modes shown in the bottom panel. The circles represent the values obtained from the measured lasing wavelength λ_{max} and the corresponding grating period Λ. The triangles represent the simulated effective refractive index using waveguide simulations for the different lasing modes.

indication for laser action. Figure 3b shows that just above threshold, at a pump pulse energy of 0.9 µJ, a weak and narrow peak starts to appear on top of the fluorescence background of eGFP. This peak grows superlinearly in intensity until it dominates the spectrum at input power energies ≥2.0 µJ. This is a further indication for lasing action from the DFB eGFP structure. The single-mode operation at 543 nm is characteristic for our DFB resonator with a grating period $\Lambda = 330$ nm; using the lasing wavelength and grating period and solving the Bragg condition ($m\lambda = 2n_{eff}\Lambda$; where λ is the vacuum wavelength and m is an integer) yields an effective refractive index of $n_{eff} \approx 1.65$ that agrees well with the calculated value (see below). We also tested the input–output characteristics of an eGFP film spin-coated directly on top of a polymer grating, that is, without the high refractive index metal oxide layer. As expected, even at high pump fluences (>2 MW cm^{-2}) we did not observe any line narrowing associated with lasing but only broad fluorescence emission, confirming that a refractive index profile without a high index interlayer does not support lasing.

The UV nanoimprint process allows transfer of extended master structures containing several gratings onto the sample in a single processing step. To characterize the effect of varying the grating period Λ, we produced a sample containing 35 different gratings with grating periods ranging from 250 to 425 nm, incrementing in $\Delta\Lambda = 5$ nm steps. Using these gratings, it was possible to tune the wavelength of lasing in eGFP over a range from 525.1 to 576.7 nm (Figure 3c). The overall wavelength range available for lasing was thus 51.6 nm. Even though the maximum emission peak of eGFP is at 510 nm, we did not observe laser action at wavelengths shorter than 525 nm. We attribute the truncation of lasing at shorter wavelengths to the onset of absorption in eGFP. In fact, the absorption peak in solid-state eGFP films extends to wavelengths ≈525 nm.[19] At the long wavelength end, laser emission ceases at 576.7 nm, which we attribute to the reduced gain provided by eGFP at longer wavelengths.

Next, we investigated the polarization of the lasers by inserting a linear polarizer into the collection arm of our optical characterization setup. This revealed that the laser action associated with

the first three peaks in Figure 3c was in the TE mode of the waveguide, whereas the five lasing peaks at longer wavelengths were in TM mode. There is a jump in grating period from 325 to 345 nm as a part of the sample was not covered with eGFP due to a spin-coating defect. With knowledge of the emission peak wavelength λ and the grating period Λ, one can use the Bragg condition to calculate the effective refractive index n_{eff} of the underlying photonic modes. The circles in the top panel of Figure 3c represent the calculated effective refractive index n_{eff} for the lasing peaks originating from each grating. Another method to determine the effective refractive index n_{eff} of a mode is by numerically computing the supported photonic modes of the given 2D dielectric waveguide using appropriate boundary conditions. Using the refractive indices from ellipsometry and thicknesses extracted from the FIB/SEM measurements, respectively, as well as the emission wavelength λ and the polarization (TE or TM), we calculated the effective refractive index values for each lasing peak (transparent triangles in Figure 3c). Overall, there is a good agreement between the experimentally obtained and modelled effective refractive index for all modes. The TE laser mode for the grating with $\Lambda = 315$ nm showed the highest discrepancy between measured and calculated effective refractive index, but even here the difference is only $\Delta n_{max} = 0.004$. We take this as evidence that we have a correct understanding and theoretical description of the DFB eGFP laser structure.

Generally, the effective refractive index is higher for TE than for TM modes. This can be attributed to the polarization of the electric field of the TE modes, which oscillates in the plane of the waveguide and hence mainly experiences the high refractive index of the metal oxide layer. Having access to both TE and TM modes from the same layer stack is unusual for solution processed DFB lasers as the conjugated polymer gain materials most widely used in these structures show strong optical anisotropy when deposited as thin films. This leads to substantial optical birefringence; a difference in refractive index of up to 0.5 between TE and TM modes has been reported for some light-emitting polymers.[20] Therefore, the effective refractive index experienced by TE and TM modes in polymer DFB lasers is generally very
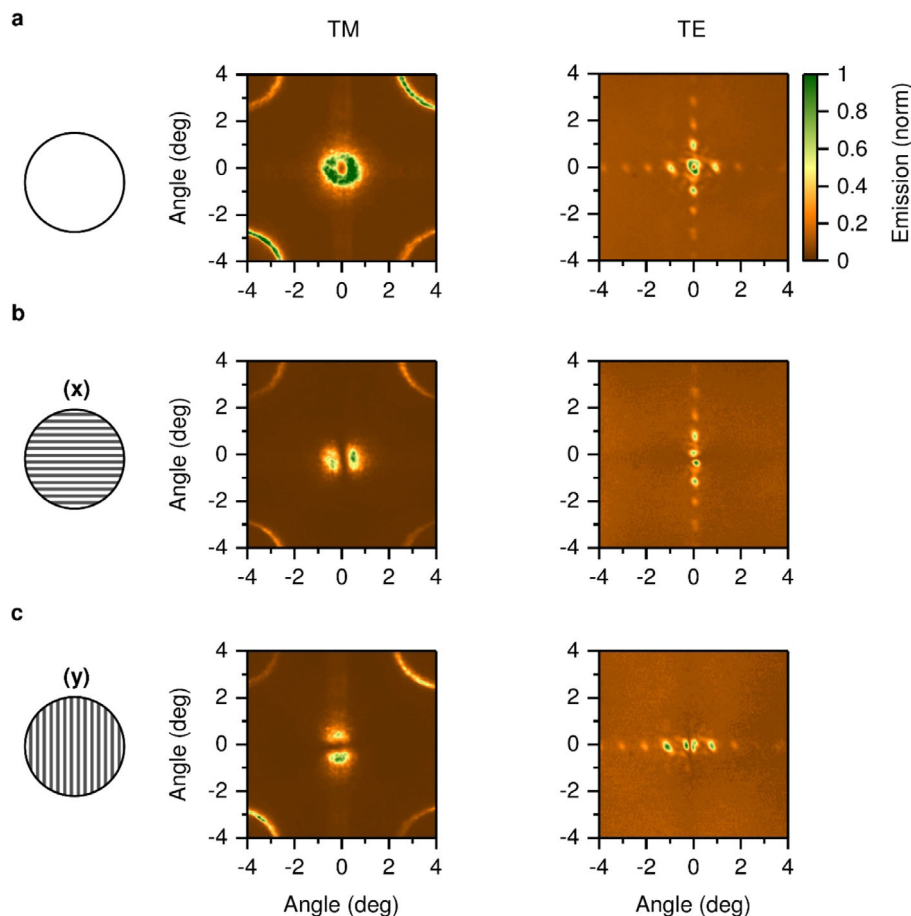
**ADVANCED
SCIENCE NEWS**

www.advancedsciencenews.com

LASER
& PHOTONICS
REVIEWS

www.lpr-journal.org

Figure 4. Far field emission of a DFB eGFP laser for a TM (left panel) and a TE (right panel) mode. a) Detected without polarization filter. b) After inserting a horizontally oriented polarization filter into the collection arm. c) Using a vertical polarization filter.

different and the Bragg condition cannot be fulfilled for both polarizations. By contrast, the "globular" molecular structure of eGFP avoids or at least substantially reduces optical anisotropy in thin films of this material.

4. Laser Beam Properties of DFB eGFP Lasers

Next, we analyzed the far-field emission profile of the beams emitted by the DFB eGFP lasers. 2D second-order DFB gratings scatter light in the direction perpendicular to the surface. **Figure 4** shows two characteristic TM and TE beams emitted from DFB eGFP lasers (collected from gratings with a period of $\Lambda = 345$ and $\Lambda = 325$ nm, respectively). These grating periods were selected as representative examples for TM and TE mode emission. Samples with different grating periods showed qualitatively similar far field emission characteristics. The emission was recorded using the same setup as before, but instead of using an EM-CCD detector attached to a spectrograph, we imaged the emission directly onto a CCD camera using an additional Fourier lens and projection lens. For both gratings, the emission featured an annular transverse mode originating from a 2D Bloch resonance.[21] The creation of this resonance can be explained by the 2D confinement leading to a superposition of the

two orthogonally oriented in-plane grating vectors.[22] The well-defined emission and hence spatial coherence provide additional evidence for lasing from our structures.

To analyze the properties of the emitted beams further, we imaged both beams through a linear polarizer. A double-lobed beam was observed, whose orientation depends on the orientation of the linear polarizer. We observed that the beam emitted from the grating with $\Lambda = 345$ nm was radially polarized. This can be attributed to Bragg scattering from a TM mode. In contrast, the output from the grating with $\Lambda = 325$ nm was azimuthally polarized and hence originating from a TE laser mode.

To understand the distinctive annular far-field pattern of the laser emission, we considered how the geometry of the DFB eGFP laser deviates from an idealized square grating structure of infinite size. For this ideal case, one would not expect to observe any surface emission, because the electromagnetic field distribution within the device would result in complete destructive interference between the different vertically diffracted waves. In brief, the intensity of surface emission from the grating depends on the relative phase shift between light diffracted from the different waves counterpropagating in the plane of the sample. If the Bragg condition is fulfilled and feedback is generated, the phase shift between these in-plane waves is exactly π,[23] and hence the two vertically diffracted waves interfere destructively.[24] In

reality, our device has a finite size defined by the size of the pump spot and the resulting optically active grating. Therefore, the perfect antisymmetric field distribution and resulting destructive interference are disrupted, most strongly at the edges of the optically active grating. This leads to substantial emission from the grating[21] and causes an annular shaped far-field emission pattern with destructive interference at 0° angle.[25]

5. Discussion

In summary, we have presented a novel waveguide and grating architecture which allows integration of a solid-state eGFP film as the active material of a DFB laser. By introducing a thin (≈65 nm) and high refractive index ($n = 2.12$) metal oxide core layer, we circumvented the unfavorable refractive index combination of eGFP and typical UV-NIL grating polymers. The use of ALD yielded a smooth and conformal waveguide core layer with homogenous and controlled thickness as confirmed by FIB/SEM measurements. 2D second-order DFB eGFP lasers fabricated following this strategy showed a well-defined pump threshold of 56.6 kW cm^{-2} and a wavelength tuning range of $\Delta\lambda = 51.7$ nm. Furthermore, we showed that in contrast to conventional organic DFB lasers based on conjugated polymers as optical gain material, both TE and TM modes are accessible and that the effective refractive index of the modes can be predicted accurately. Far-field imaging of the laser emission revealed a peculiar annular laser beam profile that can be attributed to the finite-size of the optically active grating.

6. Experimental Section

DFB eGFP Laser Fabrication: A thin (<10 nm) adhesion promoter (mr-APS1, Micro Resist Technology) was first spin coated on an oxygen-plasma-treated glass substrate. Subsequently, a photo-curable polymer resist (mr-NIL210, Micro Resist Technology) was spin-coated and baked according to the manufacturer's guidelines. A transparent perfluoropolyether soft stamp, comprising a negative of the final grating, was then pressed into the photo-curable polymer layer and exposed to UV light using a UV imprint alignment system (EVG620, EV Group, $\lambda = 365$ nm, dose 56 mW cm^{-2}, exposure time 220 s). The soft stamp was removed, and the grating surface was treated with an oxygen plasma to remove remaining organic residues. Next, a layer of ZrO$_2$ was deposited onto the mr-NIL210 gratings in the reaction chamber of an ALD system (Ultratech Savannah 200). Two precursors, tetrakis(dimethylamino)zirconium (Pegasus Chemicals) and water, were alternately purged into the reaction chamber at a deposition temperature of 100 °C.[26] Under these conditions, ZrO$_2$ grew at a rate of 55 Å h^{-1}. A combination of ellipsometry and profilometer measurements was used to determine the refractive index ($n = 2.12$) and thickness (65 nm) of the deposited ZrO$_2$ layer. Lastly, an aqueous eGFP solution was spin-cast onto the ZrO$_2$ layer (spin coating: 1500 rpm for 120 s; concentration: 100 × 10^{-3} M; volume: 40 µL), yielding a solid-state eGFP film with a thickness of ≈1 µm.

Optical Characterization: The DFB eGFP lasers were investigated on a custom-built inverted fluorescence microscope. Excitation pulses produced with an OPO (Opolette 355, Opotek, Inc.) tuned to the absorption maximum of eGFP at 490 nm (pulse duration: 5 ns; repetition rate: 20 Hz) were passed through a dichroic beam splitter and focused onto the bottom of the sample using a 10× microscope objective. The emission from the DFB eGFP lasers was collected with the same microscope objective and passed into the collection arm. The light was spectrally resolved by focusing it onto the entrance slit of a spectrograph (Shamrock 500i,

Andor) and recording the signal on an EM-CCD camera (Newton 971, Andor) attached to the spectrograph.

Far field emission measurements were recorded with a separate CCD camera by imaging the back focal plane of the objective.

To control the pump power density of single pulses and to record the input–output characteristics of the DFB eGFP lasers, the OPO emission was passed through a set of different computer-controlled optical density filters. The emission spectra at different pump power densities were recorded and spectrally integrated to determine the lasing threshold.

Conflict of Interest

The authors declare no conflict of interest.

[1] M. Chalfie, Y. Tu, G. Euskirchen, W. W. Ward, D. C. Prasherf, *Science* **1992**, *263*, 802.

[2] E. Betzig, G. H. Patterson, R. Sougrat, O. W. Lindwasser, S. Olenych, J. S. Bonifacino, M. W. Davidson, J. Lippincott-Schwartz, H. F. Hess, *Science* **2006**, *313*, 1642.

[3] N. C. Shaner, P. A. Steinbach, R. Y. Tsien, *Nat. Methods* **2005**, *2*, 905.

[4] N. C. Shaner, R. E. Campbell, P. A. Steinbach, B. N. Giepmans, A. E. Palmer, R. Y. Tsien, *Nat. Biotechnol.* **2004**, *22*, 1567.

[5] M. C. Gather, S.-H. Yun, *Nat. Commun.* **2014**, *5*, 5722.

[6] R. Xia, G. Heliotis, D. D. C. Bradley, *Appl. Phys. Lett.* **2003**, *82*, 3599.

[7] M. C. Gather, S. H. Yun, *Nat. Photon.* **2011**, *5*, 406.

[8] C. P. Dietrich, A. Steude, L. Tropf, M. Schubert, N. M. Kronenberg, K. Ostermann, S. Höfling, M. C. Gather, *Sci. Adv.* **2016**, *2*, e160666.

[9] F. Hide, M. A. Díaz-García, B. J. Schwartz, M. R. Andersson, A. J. Heeger, *Science* **1996**, *273*, 1833.

[10] V. G. Kozlov, V. Bulović, P. E. Burrows, S. R. Forrest, *Nature* **1997**, *389*, 362.

[11] N. Tessler, G. J. Denton, R. H. Friend, *Nature* **1996**, *382*, 695.

[12] I. B. Dogru, K. Min, M. Umar, H. B. Jalali, E. Begar, D. Conkar, E. N. F. Karalar, S. Kim, S. Nizamoglu, *Appl. Phys. Lett.* **2017**, *111*, 231103.

[13] S. M. George, *Chem. Rev.* **2010**, *110*, 111.

[14] R. W. Johnson, A. Hultqvist, S. F. Bent, *Mater. Today* **2014**, *17*, 236.

[15] J. S. Park, H. Chae, H. K. Chung, S. I. Lee, *Semicond. Sci. Technol.* **2011**, *26*, 034001.

[16] M. Knez, K. Nielsch, L. Niinistö, *Adv. Mater.* **2007**, *19*, 3425.

[17] W. Song, A. E. Vasdekis, Z. Li, D. Psaltis, *Appl. Phys. Lett.* **2009**, *94*, 161110.

[18] M. Karl, G. L. Whitworth, M. Schubert, C. P. Dietrich, I. D. W. Samuel, G. A. Turnbull, M. C. Gather, *Appl. Phys. Lett.* **2016**, *108*, 261101.

[19] J. M. Zajac, M. Schubert, T. Roland, C. Keum, I. D. W. Samuel, M. C. Gather, *Adv. Funct. Mater.* **2018**, *28*, 1706300.

[20] B. L. Lachut, S. A. Maier, H. A. Atwater, M. J. A. de Dood, A. Polman, R. Hagen, S. Kostromine, *Adv. Mater.* **2004**, *16*, 1746.

[21] Y. Liang, C. Peng, K. Sakai, S. Iwahashi, S. Noda, *Opt. Express* **2012**, *20*, 15945.

[22] J. R. Harwell, G. L. Whitworth, G. A. Turnbull, I. D. W. Samuel, *Sci. Rep.* **2017**, *7*, 11727.

[23] E. Miyai, S. Noda, *Appl. Phys. Lett.* **2005**, *86*, 111113.

[24] Y. Liang, C. Peng, K. Sakai, S. Iwahashi, S. Noda, *Phys. Rev. B* **2011**, *84*, 195119.

[25] R. F. Kazarinov, C. H. Henry, *IEEE J. Quantum Electron.* **1985**, *21*, 144.

[26] J. Li, C.-X. Huang, J.-H. Zhang, *RSC Adv.* **2017**, *7*, 52517.